
9 VISCOELASTIC EFFECTS IN 3D MICROPHASE SEPARATION OF BLOCK COPOLYMERS

This chapter was submitted as:

'Viscoelastic effects in 3D microphase separation of block copolymers.

Dynamic mean-field density functional approach'.

N.M. Maurits, A.V. Zvelindovsky, J.G.E.M. Fraaije,

Journal of Chemical Physics, 1998.

9.1 Summary

In the present paper, we extend the dynamic mean-field density functional method which describes microphase separation phenomena in polymer liquids, to account for viscoelastic effects. The effect of simple steady shear on polymer orientation and elongation is taken into account by adapting the polymer configurational distribution function. We propose a simplified model for polymer chains in a simple steady shear flow and show numerically that this model correctly reproduces expected conformational changes. The conformational effect is only of importance for high viscosity liquids and/or high shear rates.

9.2 Introduction

General

Non-Newtonian fluids, such as complex polymer liquids, show unusual flow behaviour in the form of e.g. shear-thinning (decreasing viscosity with increasing shear rate) and normal stress effects (die-swell and rod-climbing). An important problem in rheology is to understand these phenomena from the microscopic properties of the material. Heuristically, shear-thinning behaviour can be explained as follows. If a polymer liquid is at rest, the polymers are random coil and the mobility of the constituting molecules is limited. If a simple steady shear flow is applied, the large polymer molecules align and orient with the flow direction, making it easier for the constituting molecules to flow past each other,

thereby effectively lowering the viscosity. The behaviour of the liquid in response to a simple steady shear, defines its viscosity $\eta(\dot{\gamma})$ ^{191,197} as the ratio between the shear stress τ_{12} and the shear rate $\dot{\gamma}$: $\tau_{12} = \eta(\dot{\gamma})\dot{\gamma}$. For complex liquids, the viscosity is in principle shear rate dependent. The heuristic explanation for shear-thinning behaviour above shows that in order to be able to understand and represent rheological phenomena in complex liquids from the microscopic detail of the material using the dynamic mean-field density functional method,²⁸ at least the effect of macroscopic flow should be included.³⁷ A question that has already been answered in a previous publication¹⁹⁸ is how to calculate the stress tensor $\sigma_{\alpha\beta}$. In the present paper, we will also show how an external flow influences the stress tensor in an inhomogeneous polymer liquid. The stress tensor gives access to mechanical properties of a(n) (in)homogeneous material via the constitutive equation which relates the stress tensor to the velocity gradient tensor $\kappa_{\alpha\beta}$. It is known that in polymeric liquids,³⁷ the stress is mainly due to intramolecular force and directly related to the polymer orientation. This provides another reason which makes it important to account for polymer orientation and elongation due to an externally applied steady simple shear field. Currently in the dynamic mean-field density functional theory,²⁸ the polymer chains do not respond to externally applied flows, although their macroscopic response to simple steady shear correctly reproduces experimental results.^{10,199}

Until now, most theory to describe viscoelastic effects has been developed for liquids with slowly relaxing fluctuations such as liquids near the critical point and entangled polymers, for phase separating liquids such as amphiphilic (A/B/AB) systems and for viscoelastic two-component liquids such as polymer solutions, in which a dynamic coupling between stress and diffusion due to different viscoelastic properties takes place.¹⁹⁰ Shear effects in liquids with complex internal structures such as block copolymers have also been investigated using a phenomenological approach, both theoretically^{196,200,201} and numerically in 2D.^{149,150} The first 3D simulations of a block copolymer system under shear based on the dynamic mean-field density functional method were performed recently.^{10,199} Until now, viscoelastic effects in sheared copolymer systems (such as polymer orientation and elongation due to the flow) have not explicitly been taken into account although it may be an important factor in explaining shear-thinning effects. In the present paper we take the influence of shear flow on polymer orientation into account by adapting the polymer configurational distribution function.

The effects of shear on polymeric (binary) systems (such as enhanced turbidity²⁰² or the shear-induced spinodal shift²⁰³⁻²⁰⁵) have been studied by application of a dynamic coupling mechanism,^{204,206} by incorporating a conformation tensor as an independent variable into a Ginzburg-Landau scheme^{203,207} and by computer simulations^{208,209} that employ a two-fluid model^{193,204,206} to incorporate the dynamic stress-diffusion coupling, and a viscoelastic Ginzburg-Landau free energy.²⁰⁷ Many of these models provide a combination of a model **H** type mass/momentum

balance,²¹ combined with a dynamic model for the stress or conformation tensor (e.g. upper convected Maxwell), a (linear) stress-strain relation and a Ginzburg-Landau free energy augmented with an elastic energy term.²¹⁰ In Ref. 211 various properties of dilute polymer solutions under steady shear are studied theoretically and calculated using non-equilibrium molecular and Langevin dynamics. An order-disorder transition is observed at very high shear rates and the strong effect of shear on polymer orientation and elongation is reproduced.

In the present paper, we study viscoelastic effects in 3D microphase separation in block copolymer melts using the dynamic mean-field density functional approach. This approach provides a bridge between molecular properties and mesoscopic phase separation behaviour. In macroscopic viscoelastic flow modeling other methods are also used to couple microscopic polymer properties to macroscopic (homogeneous) flow behaviour. The polymer contribution to the stress is in these cases determined by a closed-form constitutive equation such as an Oldroyd-B or (upper convected) Maxwell model, which is measured from material responses to well-defined deformations.¹⁴² However, for these closed-form models, discrepancies are found between calculations and experiments and several bypasses for constitutive equations have been invented. Finite element techniques are combined with Brownian dynamics simulations in the CONFFESSIT approach in Ref. 212 and with the dynamics of Brownian configuration fields in Ref. 213. Both techniques allow for calculations of fluid flows using polymer models for which no closed-form constitutive equation is known. Unfortunately, this approach is not straightforwardly applicable to the dynamic mean-field density functional method. Instead, we model the influence of an external shear flow on the polymer orientation and elongation by direct adjustment of the configurational distribution function.

Dynamic mean-field density functional theory

The dynamic mean-field density functional theory^{7,28} models the behaviour of complex liquids by combining Gaussian mean-field statistics with a coarse-grained Ginzburg-Landau model for time-evolution of conserved order parameters. In contrast to traditional phenomenological free energy expansion methods²⁵⁻²⁷ the free energy is not truncated at a certain level. Instead the full polymer path integral is retained by employing numerical algorithms.^{28,68,109} Recently, other groups have also started to use this approach.^{32,33} Although the repeated calculation of the polymer path integral is computationally very intensive, this approach allows for a description of the mesoscopic dynamics of *specific* complex liquids without constantly adjusting the parameters. Changes in the molecular properties are immediately reflected in the free energy, which allows for practical application of the method.

In the dynamic mean-field density functional approach a polymer

solution is modeled as a compressible system of ideal Gaussian chain molecules. The free energy functional is derived on the basis of principles from thermodynamics and statistical mechanics and consists of an internal energy term (the ensemble average of the intrachain Hamiltonian), an entropy term (the ensemble average of $\ln \Psi$ where Ψ is the configurational distribution function) and interchain interaction terms. Assuming that the system can be observed on a coarse-grained time scale such that the distribution function is always optimal and hence the free energy always minimal, the free energy functional is then optimized over all Ψ under the constraint that the density that is observed in the system is the ensemble average of a microscopic density operator. The optimal *single-chain* configurational distribution function for a Gaussian chain Hamiltonian is then given by:²⁸

$$\psi = \frac{1}{\phi} e^{-\frac{3}{2a^2} \sum_{s=2}^N (\mathbf{R}_s - \mathbf{R}_{s-1})^2 - \beta \sum_{s'=1}^N U_s(\mathbf{R}_s)} \quad (9.1)$$

where ϕ is the intramolecular partition function, a is the Gaussian bond length parameter, $\beta^{-1} = k_B T$ and N is the number of beads in the chain. The external potentials U_I are conjugate to the density fields ρ_I via the Gaussian chain density functional and are introduced in the optimization of the free energy under constraint as Lagrange multiplier fields. The free energy functional is then derived to be:^{28,109}

$$\begin{aligned} F[\{\rho_I\}] &= -kT \ln \frac{\phi^n}{n!} - \sum_I \int_V U_I(\mathbf{r}) \rho_I(\mathbf{r}) d\mathbf{r} \\ &+ \frac{1}{2} \sum_{IJ} \int_{V^2} \epsilon_{IJ} (|\mathbf{r} - \mathbf{r}'|) \rho_I(\mathbf{r}) \rho_J(\mathbf{r}') d\mathbf{r} d\mathbf{r}' \\ &+ \frac{\kappa_H}{2} \int_V \left(\sum_I \nu_I (\rho_I(\mathbf{r}) - \rho_I^0) \right)^2 d\mathbf{r}, \end{aligned} \quad (9.2)$$

where n is the number of polymer molecules, I is a component index and V is the system volume. The average density is ρ_I^0 and ν_I is the bead volume. The cohesive interactions between chains have kernels $\epsilon_{IJ} \propto \epsilon_{IJ}^0 \exp[-3/(2a^2)(\mathbf{r} - \mathbf{r}')^2]$ where ϵ_{IJ}^0 is a constant interaction parameter and κ_H is the Helfand compressibility parameter.¹⁰⁹ Notice that the same single-chain configurational distribution function (Eq. (9.1)) is found if the Smoluchowski equation for the time evolution of the configurational bead distribution function of a bead-spring system (a Gaussian chain) under an external constraining field is solved (see e.g. Refs. 37 and 142).

9.3 Viscoelastic effects

Suppose we consider the bead-spring or Gaussian chain in solution. The influence of an external flow field on the orientation of the chain can most easily be included via the single-chain configurational distribution

function ψ which depends on the positions $\mathbf{R}_1 \cdots \mathbf{R}_N$ of all beads in the chain and time t . In principle the time evolution of the distribution function ψ is described by a Smoluchowski equation.^{37,142} For a good description of linear viscoelastic phenomena, the Rouse description for 'freely draining' chains suffices. In this case, the mobility matrix is simply diagonal¹³³ and no hydrodynamic interaction between the beads in one chain is taken into account.

The flow fields that are considered in this paper are homogeneous. The positional dependence of the velocity gradient tensor $\kappa_{\alpha\beta}$ can be eliminated because the stress at a certain fluid element only depends on previous values of the velocity gradient evaluated at that same fluid element. In this case it can be assumed that:³⁷

$$\mathbf{v}_\alpha(\mathbf{r}, t) = \kappa_{\alpha\beta}(t)\mathbf{r}_\beta \quad (9.3)$$

where \mathbf{v} is the velocity field and α and β are Cartesian components. The assumption of a homogeneous velocity field is reasonable except in cases when the velocity gradient changes considerably over distances of the order of the radius of gyration of the polymer molecules. Homogeneous velocity fields are rather general and include simple steady shear flows and potential flows.

Instead of keeping the coordinates $\mathbf{R}_1 \cdots \mathbf{R}_N$, the system is described in terms of the center of mass and the connector vectors $\mathbf{Q}_k = \mathbf{R}_{k+1} - \mathbf{R}_k$.¹⁴² For a homogeneous system and a bead-spring model, the Smoluchowski equation for a single bead-spring chain in an external flow can be expressed in terms of connector vectors only:¹⁴²

$$\frac{\partial \psi}{\partial t} = - \sum_j \left(\frac{\partial}{\partial \mathbf{Q}_j} \cdot \left\{ [\kappa \mathbf{Q}_j] \psi - \frac{1}{\xi} \sum_k A_{jk} \left[k_B T \frac{\partial}{\partial \mathbf{Q}_k} \psi + F_k^{(c)} \psi \right] \right\} \right) \quad (9.4)$$

Here, ξ is the friction coefficient, the A_{ij} are elements of the Rouse matrix (2 on the diagonal, -1 on the super-/sub-diagonal and 0 elsewhere), $\mathbf{B}_{j\nu} = \delta_{j+1,\nu} - \delta_{j\nu}$ and $F_k^{(c)} = \frac{3}{\beta a^2} \mathbf{Q}_k$ for the Gaussian chain.

For the Rouse model and Gaussian chains, the solution to the Smoluchowski equation (9.4) is known for *any* homogeneous flow field. The solution is found by introducing normal coordinates \mathbf{Q}'_j to decouple the equations for the different connector vectors and postulating that the distribution function ψ is a product of functions ψ_k that depend on single decoupled coordinates. Here $\mathbf{Q}_k = \sum_j \Omega_{kj} \mathbf{Q}'_j$ where Ω is an orthonormal matrix that diagonalizes the Rouse matrix.¹⁴² This procedure leads to $N - 1$ equations in one coordinate that are solved using Fourier transforms.^{142,214} In normal coordinates the solution reads:¹⁴²

$$\psi_j(\mathbf{Q}'_j, t) = \frac{(3/(2\pi a^2))^{\frac{3}{2}}}{\sqrt{\det \alpha_j}} e^{-(3/(2a^2))(\alpha_j^{-1} \mathbf{Q}'_j \mathbf{Q}'_j)} \quad (9.5)$$

$$\alpha_j = \mathbf{I} - \frac{1}{\lambda_j} \int_{-\infty}^t e^{-(t-t')/\lambda_j} \gamma_{[0]}(t, t') dt' \quad (9.6)$$

$$\psi(\mathbf{Q}'^{N-1}, t) = \prod_{k=1}^{N-1} \psi_k(\mathbf{Q}'_k, t) \quad (9.7)$$

where $\lambda_j = \xi/(2Ha_j)$, $H = 3/(\beta a^2)$ and $a_j = 4\sin^2\left(\frac{j\pi}{2N}\right)$ (j -th eigenvalue of the Rouse matrix). The operator $'\cdot'$ is the contraction operator for tensors which is for two-dimensional tensors \mathbf{A} and \mathbf{B} defined by $\mathbf{A} : \mathbf{B} \equiv \sum_{ij} \mathbf{A}_{ij} \mathbf{B}_{ij}$. Hence $\boldsymbol{\alpha}_j^{-1} : \mathbf{Q}'_j \mathbf{Q}'_j = \mathbf{Q}'_j{}^T \boldsymbol{\alpha}_j^{-1} \mathbf{Q}'_j$.

The finite strain tensor $\boldsymbol{\gamma}_{[0]}$ for steady simple shear flow ($\mathbf{v}_x = \dot{\gamma}y$) is given by:¹⁴²

$$\boldsymbol{\gamma}_{[0]}(t, t') = \begin{pmatrix} -\gamma^2 & \gamma & 0 \\ \gamma & 0 & 0 \\ 0 & 0 & 0 \end{pmatrix} = \begin{pmatrix} -\dot{\gamma}^2(t' - t)^2 & \dot{\gamma}(t' - t) & 0 \\ \dot{\gamma}(t' - t) & 0 & 0 \\ 0 & 0 & 0 \end{pmatrix} \quad (9.8)$$

Here γ is the shear strain. Solution (9.5) for the decoupled normalized connector vectors describes the behaviour of a dumbbell (two-bead Gaussian chain) in an external flow. The dumbbell Hamiltonian is adapted to account for the elongation and orientation of the dumbbell due to the external flow, via the tensor $\boldsymbol{\alpha}_j^{-1}$. Notice that this tensor is the identity matrix if no external flow is present.

The explicit solution to Eq. (9.4) in case of steady simple shear flow is found by inserting the expression for the finite strain tensor $\boldsymbol{\gamma}_{[0]}$ (Eq. (9.8)) in Eq. (9.5):

$$\psi_k(\mathbf{Q}'_k) = \frac{(3/(2\pi a^2))^{\frac{3}{2}}}{\sqrt{1 + \lambda_k^2 \dot{\gamma}^2}} \exp \left[-\frac{3}{2a^2 (1 + \lambda_k^2 \dot{\gamma}^2)} \left\{ q_{k1}'^2 \right. \right. \quad (9.9)$$

$$\begin{aligned} & \left. - 2\dot{\gamma} \lambda_k q_{k1}' q_{k2}' + (1 + 2\lambda_k^2 \dot{\gamma}^2) q_{k2}'^2 + (1 + \lambda_k^2 \dot{\gamma}^2) q_{k3}'^2 \right\} \\ \psi(\mathbf{Q}'^{N-1}) &= \prod_k \psi_k(\mathbf{Q}'_k) \quad (9.10) \\ &= \frac{(3/(2\pi a^2))^{\frac{3}{2}(N-1)}}{\prod_k \sqrt{1 + \lambda_k^2 \dot{\gamma}^2}} \exp \left[-\frac{3}{2a^2} \sum_{k=1}^{N-1} \frac{1}{(1 + \lambda_k^2 \dot{\gamma}^2)} \left\{ q_{k1}'^2 \right. \right. \\ & \left. \left. - 2\dot{\gamma} \lambda_k q_{k1}' q_{k2}' + (1 + 2\lambda_k^2 \dot{\gamma}^2) q_{k2}'^2 + (1 + \lambda_k^2 \dot{\gamma}^2) q_{k3}'^2 \right\} \right] \end{aligned}$$

where $\mathbf{Q}'_k = (q_{k1}', q_{k2}', q_{k3}')$. Notice that the solution to the Smoluchowski equation is, in accordance with the applied steady flow, a steady solution which no longer depends on time. Expressing this solution in terms of the original connector vectors \mathbf{Q}_k leads to a coupled system again. The coupling can easily be seen in the exponent of Eq. (9.10) if the orthonormal transformation $\mathbf{Q}_k = \sum_j \Omega_{kj} \mathbf{Q}'_k$ between the connector vectors \mathbf{Q}_k and the normal coordinates \mathbf{Q}'_k is employed. This leads to the following expression:

$$-\frac{3}{2a^2} \sum_{k=1}^{N-1} \boldsymbol{\alpha}_k^{-1} : \mathbf{Q}'_k \mathbf{Q}'_k = -\frac{3}{2a^2} \left(\overline{\mathbf{Q}}_1 \quad \overline{\mathbf{Q}}_2 \quad \overline{\mathbf{Q}}_3 \right) \quad (9.11)$$

$$\times \begin{pmatrix} (\mathbf{I} + \mathbf{P}^2)^{-1} & -(\mathbf{P}^{-1} + \mathbf{P})^{-1} & 0 \\ -(\mathbf{P}^{-1} + \mathbf{P})^{-1} & (\mathbf{I} + 2\mathbf{P}^2)(\mathbf{I} + \mathbf{P}^2)^{-1} & 0 \\ 0 & 0 & \mathbf{I} \end{pmatrix} \begin{pmatrix} \overline{\mathbf{Q}}_1^T \\ \overline{\mathbf{Q}}_2^T \\ \overline{\mathbf{Q}}_3^T \end{pmatrix}$$

Here, $\overline{\mathbf{Q}}_i$ is the $1 \times (N - 1)$ vector $(q_{1i} \ q_{2i} \ \cdots \ q_{N-1i})$ and \mathbf{P} is the $(N - 1) \times (N - 1)$ matrix given by $\frac{\dot{\gamma}\xi}{2H}\mathbf{A}^{-1}$ where \mathbf{A} is the Rouse matrix. Eq. (9.11) clearly shows that due to the externally applied shear flow field all connector vectors in the Gaussian chain are explicitly coupled in \mathbf{Q} -space. The full configurational distribution function ψ (Eq. (9.10)) can therefore not be used as such in the dynamic mean-field density functional method. In the next two sections we show how an approximation to the full configurational distribution function can be made using dumbbell properties. This approximation preserves the elongation and orientation behaviour of the configurational distribution function due to the flow.

Dumbbells

In case of a dumbbell, there are no coupled connector vectors and the density of each bead type can be calculated using an adapted stencil operation.⁶⁸ For a Hookean (Gaussian) dumbbell in a simple steady shear flow, the solution to the Smoluchowski equation for the configurational distribution function of the connector vector $\mathbf{Q}_k = \mathbf{R}_{k+1} - \mathbf{R}_k$ is given by (cf. Eq. (9.10)):

$$\begin{aligned} \psi(\mathbf{Q}, t) &= \left(\frac{3}{2\pi a^2}\right)^{\frac{3}{2}} \frac{1}{\sqrt{1 + \lambda_H^2 \dot{\gamma}^2}} \exp \left\{ -\frac{3}{2a^2} \frac{1}{1 + \lambda_H^2 \dot{\gamma}^2} \right. \\ &\times \left. \begin{pmatrix} 1 & -\lambda_H \dot{\gamma} & 0 \\ -\lambda_H \dot{\gamma} & 1 + 2\lambda_H^2 \dot{\gamma}^2 & 0 \\ 0 & 0 & 1 + \lambda_H^2 \dot{\gamma}^2 \end{pmatrix} : \mathbf{Q}\mathbf{Q} \right\} \end{aligned} \quad (9.12)$$

where λ_H is the 'Rouse relaxation time' given by $\lambda_H = \xi/(4H)$.

The usual basis operation in calculating the density in the dynamic mean-field density functional method²⁸ using a Green propagator algorithm is the so-called linkage operator σ :

$$\sigma[f](\mathbf{r}) \equiv \left(\frac{3}{2\pi a^2}\right)^{\frac{3}{2}} \int_V e^{-\frac{3}{2a^2}(\mathbf{r}-\mathbf{r}')^2} f(\mathbf{r}') d\mathbf{r}' \quad (9.13)$$

which is now replaced by the 'flow' linkage operator:

$$\sigma^{\text{flow}}[f](\mathbf{r}) \equiv \left(\frac{3}{2\pi a^2}\right)^{\frac{3}{2}} \frac{1}{\sqrt{1 + \lambda_H^2 \dot{\gamma}^2}} \int_V e^{-\frac{3}{2a^2}\boldsymbol{\alpha}^{-1}:(\mathbf{r}-\mathbf{r}')(\mathbf{r}-\mathbf{r}')} f(\mathbf{r}') d\mathbf{r}' \quad (9.14)$$

where $\boldsymbol{\alpha}$ is the matrix

$$\boldsymbol{\alpha} = \begin{pmatrix} 1 + 2\lambda_H^2 \dot{\gamma}^2 & \lambda_H \dot{\gamma} & 0 \\ \lambda_H \dot{\gamma} & 1 & 0 \\ 0 & 0 & 1 \end{pmatrix} \quad (9.15)$$

This operator determines the elongation and orientation of the dumbbell due to the externally applied flow. For easy analysis the flow linkage operator σ^{flow} is transformed to Fourier space:

$$\int_V \sigma^{\text{flow}}(f) e^{-i\mathbf{q}\cdot\mathbf{r}} d\mathbf{r} = \sigma_{\mathbf{q}}^{\text{flow}} f_{\mathbf{q}}, \quad (9.16)$$

where the Fourier multiplier $\sigma_{\mathbf{q}}^{\text{flow}}$ is given by

$$\sigma_{\mathbf{q}}^{\text{flow}} = e^{-a^2 \boldsymbol{\alpha}:\mathbf{q}\mathbf{q}/6} \quad (9.17)$$

The linkage operator σ can easily be applied on a grid mainly because the operator is isotropic. This reduces the effective number of degrees of freedom in the stencil to 4, given a certain grid size h and bond length a .⁶⁸ The nonisotropic flow linkage operator σ^{flow} however, has many more degrees of freedom. It can easily be checked that the minimum representation of σ^{flow} in Fourier space on a 27-point stencil has 9 degrees of freedom and must look as follows (in case $\mathbf{v}_x = \dot{\gamma}y$):

$$\begin{aligned} \left(\sigma_{\mathbf{q}}^{\text{flow}}\right)_{\text{grid}} &= c_0 + c_1 \cos(q_x h) + c_2 [\cos(q_y h) + \cos(q_z h)] \\ &+ c_3 \cos[(q_x + q_y)h] + c_4 \cos[(q_x - q_y)h] \\ &+ c_5 \{\cos[(q_x + q_z)h] + \cos[(q_x - q_z)h]\} \\ &+ c_6 \{\cos[(q_y + q_z)h] + \cos[(q_y - q_z)h]\} \\ &+ c_7 \{\cos[(q_x + q_y + q_z)h] + \cos[(q_x + q_y - q_z)h]\} \\ &+ c_8 \{\cos[(q_x - q_y + q_z)h] + \cos[(q_x - q_y - q_z)h]\} \end{aligned} \quad (9.18)$$

Notice that the stencil depends explicitly on the flow direction. The size of $\lambda_H \dot{\gamma}$ determines the amount of isotropy in the nonisotropic linkage operator σ^{flow} . The size of $\lambda_H \dot{\gamma} = \xi a^2 \dot{\gamma} \beta / 12$ can be roughly estimated. Realistic values for the shear rate $\dot{\gamma}$ ($1 < \dot{\gamma} < 10 \text{ s}^{-1}$), the friction coefficient ξ (10^9 (water) $< \xi \beta < 10^{13}$ (viscous liquid) m^{-2}s) and the bond length parameter a ($10^{-18} < a^2 < 10^{-14} \text{m}^2$) lead to the large range of $0.083 \times 10^{-9} < \lambda_H \dot{\gamma} < 0.083$. It is known from experiments that Rouse relaxation times can be of the order of microseconds, but also in the order of seconds. Notice that the parameter $\lambda_H \dot{\gamma}$ is very similar in nature to the Deborah number De which is well-known from rheology. The Deborah number measures the relative importance of the deformation history of the material by the ratio of the internal relaxation time and the time scale of the flow. For viscoelastic flows De is $O(1)$. In conclusion, even for very viscous polymer liquids and rather high shear rates, the deviation from the isotropic linkage operator is limited. We hence consider $\lambda_H \dot{\gamma} = 0.01$ and $\lambda_H \dot{\gamma} = 0.1$, which are on the high end of the nonisotropy scale.

The nonisotropic stencil $\left(\sigma_{\mathbf{q}}^{\text{flow}}\right)_{\text{grid}}$ can then be fitted to the nonisotropic linkage operator σ^{flow} in the following points: $(0, 0, 0)$, $(0, \frac{\pi}{2h}, 0)$, $(\frac{\pi}{2h}, 0, \frac{\pi}{2h})$, $(0, \frac{\pi}{2h}, \frac{\pi}{2h})$, $(\frac{\pi}{2h}, \frac{\pi}{2h}, \frac{\pi}{2h})$ and $(\frac{\pi}{2h}, -\frac{\pi}{2h}, \frac{\pi}{2h})$ and to the curvature in $(0, 0, 0)$ in the directions $(1, 0, 0)$, $(0, 0, 1)$ and $(1, 1, 0)$. Taking the optimal gridratio $a/h = 1.15430$ into account,⁶⁸ this leads to the following values for the coefficients:

$$\times \exp \left\{ -\frac{3}{2a^2} \left(\overline{\mathbf{Q}}_1 \quad \overline{\mathbf{Q}}_2 \quad \overline{\mathbf{Q}}_3 \right) A_{\text{GC}} \begin{pmatrix} \overline{\mathbf{Q}}_1^T \\ \overline{\mathbf{Q}}_2^T \\ \overline{\mathbf{Q}}_3^T \end{pmatrix} \right\} \quad (9.19)$$

where

$$A_{\text{GC}} = \frac{1}{(9 + \alpha^2)(1 + \alpha^2)} \quad (9.20)$$

$$\times \begin{pmatrix} 9 + 5\alpha^2 & -4\alpha^2 & -6\alpha - 2\alpha^3 & -3\alpha + \alpha^3 & 0 & 0 \\ -4\alpha^2 & 9 + 5\alpha^2 & -3\alpha + \alpha^3 & -6\alpha - 2\alpha^3 & 0 & 0 \\ -6\alpha - 2\alpha^3 & -3\alpha + \alpha^3 & 9 + 15\alpha^2 + 2\alpha^4 & 4\alpha^2 & 0 & 0 \\ -3\alpha + \alpha^3 & -6\alpha - 2\alpha^3 & 4\alpha^2 & 9 + 15\alpha^2 + 2\alpha^4 & 0 & 0 \\ 0 & 0 & 0 & 0 & (9 + \alpha^2)(1 + \alpha^2) & 0 \\ 0 & 0 & 0 & 0 & 0 & (9 + \alpha^2)(1 + \alpha^2) \end{pmatrix}$$

and $\alpha = \xi\dot{\gamma}/(2H) = 2\lambda_H\dot{\gamma}$. By taking the product of Eq. (9.12) with itself, the configurational distribution function of two noninteracting dumbbells connected in one chain that act independently with respect to the flow is found to be:

$$\begin{aligned} \psi_{\text{DB}}(\mathbf{Q}^2) &= \left(\frac{3}{2\pi a^2} \right)^3 \frac{1}{1 + \lambda_H^2 \dot{\gamma}^2} \\ &\times \exp \left\{ -\frac{3}{2a^2} \frac{1}{1 + \lambda_H^2 \dot{\gamma}^2} \left(q_{11}^2 - 2\lambda_H \dot{\gamma} q_{11} q_{12} \right. \right. \\ &+ (1 + 2\lambda_H^2 \dot{\gamma}^2) q_{12}^2 + (1 + \lambda_H^2 \dot{\gamma}^2) q_{13}^2 + q_{21}^2 - 2\lambda_H \dot{\gamma} q_{21} q_{22} \\ &- 2\lambda_H \dot{\gamma} q_{21} q_{22} + (1 + 2\lambda_H^2 \dot{\gamma}^2) q_{22}^2 + (1 + \lambda_H^2 \dot{\gamma}^2) q_{23}^2 \left. \right\} \\ &= \left(\frac{3}{2\pi a^2} \right)^3 \frac{1}{1 + \alpha^2/4} \\ &\times \exp \left\{ -\frac{3}{2a^2} \left(\overline{\mathbf{Q}}_1 \quad \overline{\mathbf{Q}}_2 \quad \overline{\mathbf{Q}}_3 \right) A_{\text{DB}} \begin{pmatrix} \overline{\mathbf{Q}}_1^T \\ \overline{\mathbf{Q}}_2^T \\ \overline{\mathbf{Q}}_3^T \end{pmatrix} \right\} \quad (9.21) \end{aligned}$$

where

$$A_{\text{DB}} = \frac{1}{1 + \alpha^2/4} \quad (9.22)$$

$$\times \begin{pmatrix} 1 & 0 & -\alpha/2 & 0 & 0 & 0 \\ 0 & 1 & 0 & -\alpha/2 & 0 & 0 \\ -\alpha/2 & 0 & 1 + \alpha^2/2 & 0 & 0 & 0 \\ 0 & -\alpha/2 & 0 & 1 + \alpha^2/2 & 0 & 0 \\ 0 & 0 & 0 & 0 & 1 + \alpha^2/4 & 0 \\ 0 & 0 & 0 & 0 & 0 & 1 + \alpha^2/4 \end{pmatrix}$$

The two configurational distribution functions ψ_{DB} (for two noninteracting dumbbells that act independently with respect to the flow) and ψ_{GC} (for a 3-bead Gaussian chain that acts in its totality with respect to the flow) differ only in the matrices A_{DB} and A_{GC} and a prefactor. For the largest value of α that is of interest to us ($\alpha = 0.2$), the matrices A_{GC} and A_{DB} are given by:

$$A_{\text{GC}} = \begin{pmatrix} 0.9786 & -0.017 & -0.1293 & -0.063 & 0 & 0 \\ -0.017 & 0.9786 & -0.063 & -0.1293 & 0 & 0 \\ -0.129 & -0.063 & 1.0214 & 0.017 & 0 & 0 \\ -0.063 & -0.129 & 0.017 & 1.0214 & 0 & 0 \\ 0 & 0 & 0 & 0 & 1 & 0 \\ 0 & 0 & 0 & 0 & 0 & 1 \end{pmatrix} \quad (9.23)$$

and

$$A_{\text{DB}} = \begin{pmatrix} 0.99 & 0 & -0.099 & 0 & 0 & 0 \\ 0 & 0.99 & 0 & -0.099 & 0 & 0 \\ -0.099 & 0 & 1.0099 & 0 & 0 & 0 \\ 0 & -0.099 & 0 & 1.0099 & 0 & 0 \\ 0 & 0 & 0 & 0 & 1 & 0 \\ 0 & 0 & 0 & 0 & 0 & 1 \end{pmatrix} \quad (9.24)$$

This shows that approximating the 3-bead Gaussian chain by two noninteracting dumbbells connected in one chain that act independently with respect to the flow, implies that the coupling between the two connector vectors due to the flow is neglected as might be expected. Also, the orientation of one of the connector vectors with respect to the flow is smaller for the two dumbbells than for the Gaussian chain because the orientation is not enhanced by coupling. As a first step towards incorporating the (viscoelastic) effects of flow in the dynamic mean-field density functional method, the approach seems justified however.

Notice that the dumbbell model is special in the sense that it is one of the few polymer models for which a closed-form constitutive equation (upper convected Maxwell model) can be derived.¹⁴² However, in the approach taken here, we attempt to include the influence of the flow on polymer orientation directly in the configurational distribution function, instead of extending the dynamics equations with an extra equation for the stress tensor. Moreover, the stress tensor also changes in a thermodynamic sense because of the adapted distribution function, compared to Ref. 198. The expression for the stress tensor can again be evaluated using the principle of virtual work. Instead of completely deriving the expression for the stress tensor taking the adapted configurational distribution function into account, we just show the result for the (thermodynamic) pressure:

$$\begin{aligned} p &\equiv -\frac{1}{3}(\sigma_{xx} + \sigma_{yy} + \sigma_{zz}) \\ &= \frac{nN}{\beta V} - \frac{2n}{3V} \left\langle \frac{3}{2\beta a^2} \sum_{s=2}^N \boldsymbol{\alpha}^{-1} : (\mathbf{R}_s - \mathbf{R}_{s-1})(\mathbf{R}_s - \mathbf{R}_{s-1}) \right\rangle + p^{nid} \end{aligned}$$

The nonideal part of the pressure does by definition not depend on the distribution function and is hence exactly the same as previously derived in Ref. 198. The ensemble average $\langle \cdot \rangle$ has to be taken with respect to the adapted configurational distribution function. Clearly the expression for the ideal pressure still consists of an 'ideal gas' contribution and a contribution due to the ideal Hamiltonian.

9.4 Numerical results

In order to study viscoelastic effects using the dumbbell approximation to the Gaussian chain as described in the previous section, we have per-

formed numerical simulations of the dynamic mean-field density functional method. Notice that the solution to the Smoluchowski equation for a Gaussian chain in a simple steady shear field and the approximate viscoelastic model are derived for a *homogeneous* system. However, since the external potential field U , that acts as a constraint on the densities,²⁸ only depends on bead coordinates it is not explicitly influenced by the applied shear flow. It can be shown that the expression for the free energy (9.2) is not changed by the change in the distribution function, except that it has to be evaluated with respect to the new distribution function. The density functional itself is also changed of course. The optimization procedure for the free energy of an *inhomogeneous* system as described in Ref. 28 does not explicitly depend on the precise form of the ideal Hamiltonian H^{id} . The expression for the free energy in terms of the single-chain distribution function assumes that H^{id} factorizes in single-chain Hamiltonians. This assumption remains valid for the adapted configurational distribution function. The only change in the numerical procedure is that the adapted stencil for the flow linkage operator is used.

We have studied an A_8B_8 diblock copolymer melt under simple steady shear. The dimensionless interaction parameters are $\beta\epsilon_{AA}^0/\nu = \beta\epsilon_{BB}^0/\nu = 0.0$ and $\beta\epsilon_{BB}^0/\nu = 1.0$. The dimensionless compressibility parameter is $\beta\kappa_H\nu = 30.0$. All mobility coefficients M and molecular volumes ν are identical. The dimensionless densities $\theta_I = \nu\rho_I$ are integrated numerically by a Crank-Nicolson scheme on a $32 \times 32 \times 32$ cubic grid for 1000 dimensionless time steps $\Delta\tau = \beta^{-1}Mh^{-2}\Delta t$ without shear. Here h is the grid size and Δt is the discretized time step. All other parameters and details on the numerical integration can be found in Refs. 22 and 28. After $\tau = 1000$ the melt is sheared: $\mathbf{v}_x = \dot{\gamma}y$ in which $\dot{\gamma}$ is the shear rate. We have performed two simulations in which the dimensionless shear rate $\tilde{\gamma} = 0.01$ and two simulations in which $\tilde{\gamma} = 0.02$. In the first case the simulation box is shifted 0.32 grid cells per time step, in the second case the simulation box is shifted 0.64 grid cells per time step. For each value of $\tilde{\gamma}$ we have performed a simulation in which the configurational distribution function is the same as in earlier simulations and a simulation in which the configurational distribution function is adapted (using $\dot{\gamma}\lambda_H = 0.01$ and $\dot{\gamma}\lambda_H = 0.1$ for $\tilde{\gamma} = 0.01$ and $\tilde{\gamma} = 0.02$ respectively) to take the externally applied flow field into account as in the dumbbell model (see Section 9.3.b).

As can be concluded from Fig. 9.1, there is a global effect on the morphology if the adapted configurational distribution function is taken into account. Even though the system is simulated for a longer period (10700 time steps instead of 10000), it is not yet equilibrated (Fig. 9.1b). Notice that the overall orientation is not significant in these small boxes. The influence of the periodic boundary conditions is considerable. If the system in Fig. 9.1a is simulated in a $64 \times 64 \times 64$ cubic box, the orientation becomes more perpendicular (unpublished results). Apparently, the small changes in the density evolution due to the adapted configurational distribution function, give rise to a different preferred orientation

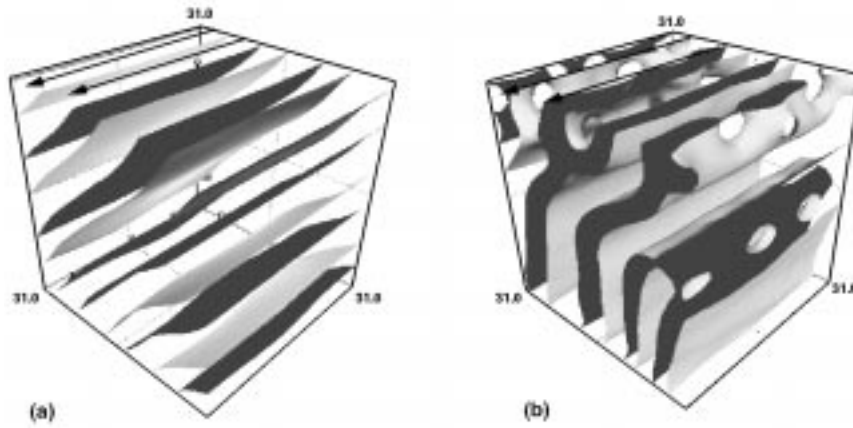


Figure 9.1 Isosurface representations of the A_8B_8 diblock copolymer melt for $\theta_A = 0.5$, $\tilde{\gamma} = 0.01$. The arrows indicate the direction of the shear. (a) Snapshot of the simulation box at $\tau = 10000$ for the simulation with the original configurational distribution function. (b) Snapshot of the simulation box at $\tau = 10700$ for the simulation with the adapted configurational distribution function, $\dot{\gamma}\lambda_H = 0.01$.

in this *small* system. Moreover, for a proper representation of preferred morphologies under shear, different viscosities should be included in the simulation (see also Ref. 10). Since the lamellae in Fig. 9.1b are oriented more or less perpendicular, the possible effect of thinning of lamellae if the polymers orient with the flow is not visible.

To analyze the influence of the dumbbell viscoelastic model on the actual polymer orientation, we have performed a conformational analysis. Although individual polymers can not be distinguished in the dynamic mean-field density functional method, a conformation analysis can give the most probable position of beads given that one of the beads in the chain is fixed at a certain position. The middle A-bead is fixed at a position in the middle of an A-lamella which is closest to being parallel to the shear, so that the effect of the model on polymer orientation can be best observed. The isosurfaces of the probability density as indicated in Fig. 9.2 are more or less as expected. The probability of finding a B-bead given that the middle A-bead is fixed in the middle of an A-lamella, is high in the neighboring B-lamellae. The other A-beads are most probably in the A-lamella itself.

In order to be able to see whether the polymers really orient with respect to the flow, we have also calculated a conformational analysis taking the original configurational distribution function into account. The position of the fixed A-bead remains the same. As can be concluded from Fig. 9.3 the most probable polymer orientation is slightly tilted in the direction of the flow for the viscoelastic dumbbell model. This orientation can not be observed in Fig. 9.3b. In Fig. 9.3c an isosurface is plotted of the difference between the two B-bead probability isosurfaces in Figs.

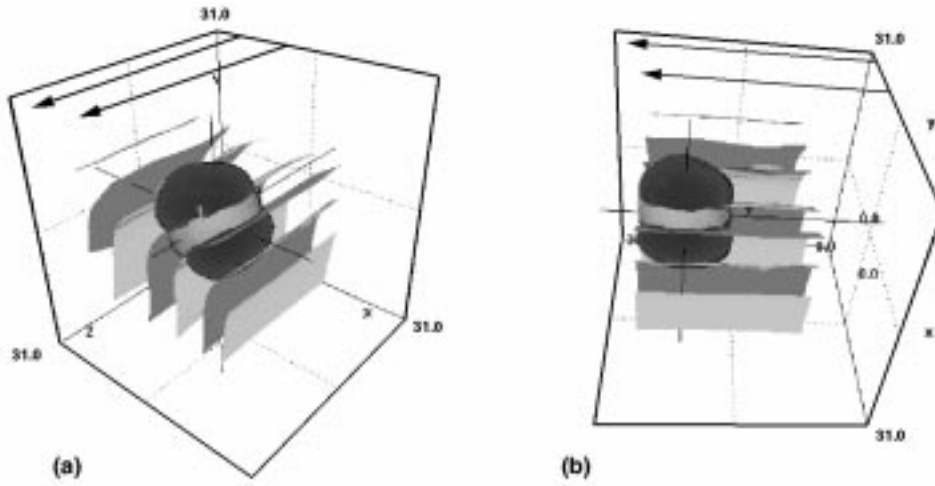


Figure 9.2 Cropped isosurface for $\theta_A = 0.5$, $\tilde{\gamma} = 0.01$, $\dot{\gamma}\lambda_H = 0.01$ at $\tau = 10700$. The arrows indicate the direction of the shear. The A-bead which is closest to the B-beads was fixed at discrete position $(x, y, z) = (19, 20, 22)$ (indicated by the origin of the axes) in the middle of an A-lamella. The probability to find an A-bead or B-bead at a certain position given that this A-bead is fixed, is indicated. The rounded isosurface is the boundary of the volume in which the probability to find a B-bead is higher than $1/6$, the disk-like isosurface is the boundary of the volume in which the probability to find an A-bead is higher than $1/6$. (a) Front view. (b) Perpendicular (with respect to shear direction) view.

9.3a and 9.3b. For this simulation at low shear rate we conclude that the difference in orientation is present, but small as expected.

The results for the simulations at the higher shear rate of $\tilde{\gamma} = 0.02$ are in Figs. 9.4, 9.5 and 9.6. Although the simulation for the viscoelastic dumbbell model (Fig. 9.4b) is only half as long as the simulation using the original configurational distribution function (Fig. 9.4a), lamellae can be clearly observed which makes a conformational analysis feasible. Notice that the preferred orientation of the morphology at this high shear rate in the *small* simulation box is parallel with respect to the shear.

We have again performed the conformational analysis by fixing an A-bead at a position in the middle of an A-lamella which is closest to being parallel to the shear. The probability of finding a B-bead given that the middle A-bead is fixed in the middle of an A-lamella, is again high in the neighboring B-lamellae. The other A-beads are again most probably in the A-lamella itself.

More detailed conclusions can be derived from the results in Fig. 9.6. The effect of polymer orientation is, according to our analytical derivations, expected to be bigger in this simulation at high shear rate ($\dot{\gamma}\lambda_H$ is ten times higher than in the simulation at low shear rate). The difference is only very small however. The isosurface in Fig. 9.6c is only slightly bigger than the isosurface in Fig. 9.3c.

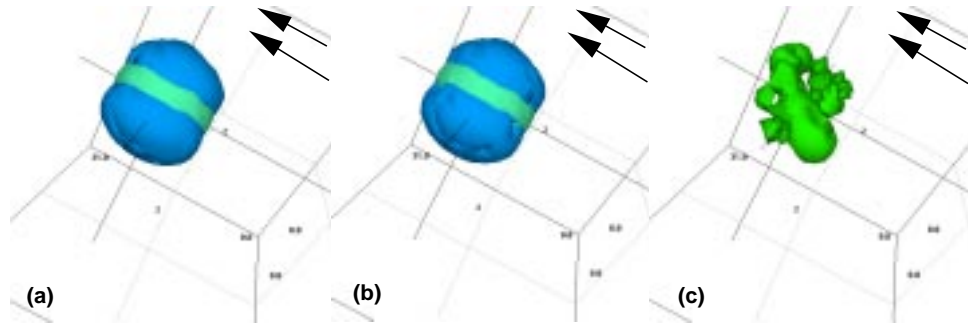


Figure 9.3 Probability isosurfaces. (a) Same isosurface as in Fig. 9.2. (b) Probability isosurface as in Fig. 9.2., except that it was calculated with respect to the original distribution function. (c) Isosurface of the difference between the two B-bead probabilities in Fig. 9.3.a and Fig. 9.3.b. Indicated is a 3 percent deviation. Larger deviations are infrequent.

9.5 Discussion and conclusion

In this paper, the dynamic mean-field density functional method is extended to account for viscoelastic effects. The effect of simple steady shear on polymer orientation and elongation is taken into account by adapting the polymer configurational distribution function. We derived a simplified model for polymer chains in a simple steady shear flow, based on the solution to the full Smoluchowski equation for the configurational distribution function of a Gaussian chain in homogeneous flow. A number of numerical simulations were performed on a diblock copolymer melt which show that the proposed model correctly reproduces expected conformational changes in a qualitative sense. The conformational effect is small, even for the high viscosity liquids and/or high shear rates that are studied in this paper. The effect increases with increasing shear rates and viscosities. The small changes in the density evolution due to the adapted configurational distribution function, give rise to different orientations in *small* simulation systems. The effect of shear-thinning can not be observed clearly from the present results. However, based on the present results we expect that in large simulation boxes in which the periodic boundary effect is negligible, shear-thinning can be reproduced provided that the system is well-equilibrated. It may be important in this respect, to account for different viscosities of chain beads.

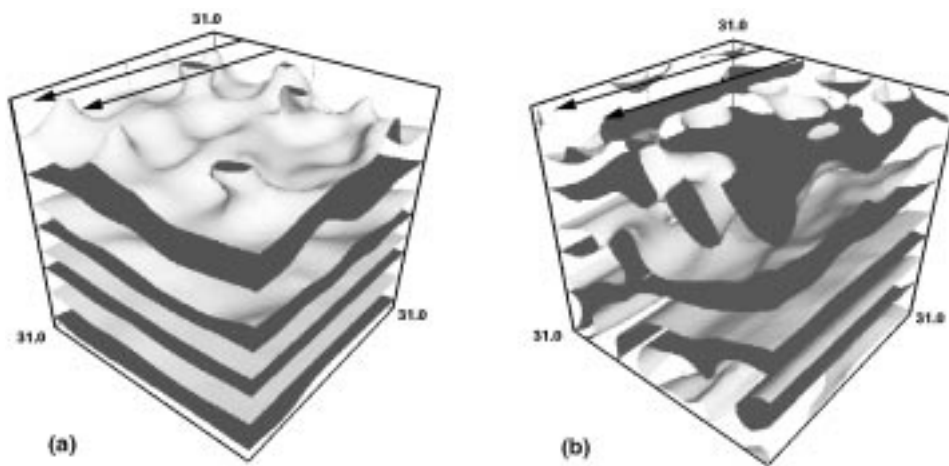


Figure 9.4 Isosurface representations of the A_8B_8 diblock copolymer melt for $\theta_A = 0.5$, $\tilde{\gamma} = 0.02$. The arrows indicate the direction of the shear. (a) Snapshot of the simulation box at $\tau = 40000$ for the simulation with the original configurational distribution function. (b) Snapshot of the simulation box at $\tau = 18350$ for the simulation with the adapted configurational distribution function, $\dot{\gamma}\lambda_H = 0.1$.

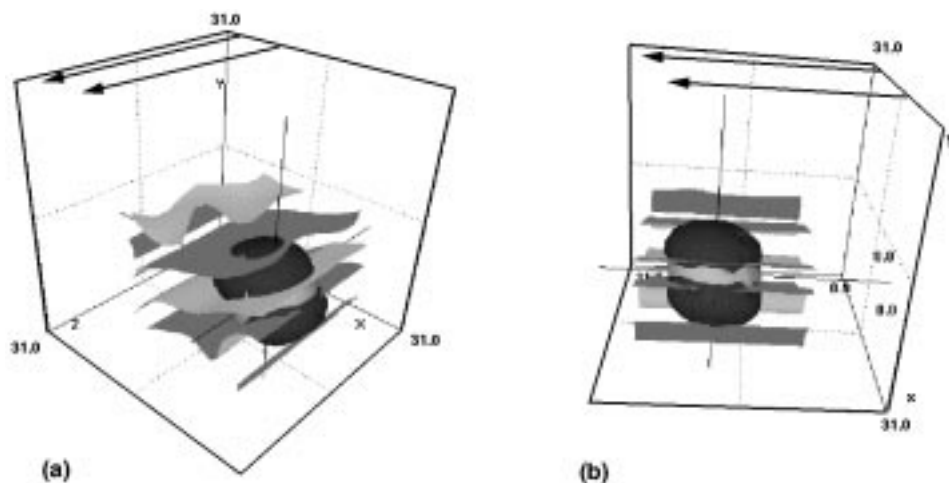


Figure 9.5 Cropped isosurface for $\theta_A = 0.5$, $\tilde{\gamma} = 0.02$, $\dot{\gamma}\lambda_H = 0.1$ at $\tau = 18350$. The arrows indicate the direction of the shear. The A-bead which is closest to the B-beads was fixed at discrete position $(x, y, z) = (24, 12, 19)$ (indicated by the origin of the axes) in the middle of an A-lamella. The probability to find an A-bead or B-bead at a certain position given that this A-bead is fixed, is indicated. The rounded isosurface is the boundary of the volume in which the probability to find a B-bead is higher than $1/6$, the disk-like isosurface is the boundary of the volume in which the probability to find an A-bead is higher than $1/6$. (a) Front view. (b) Perpendicular (with respect to shear direction) view.

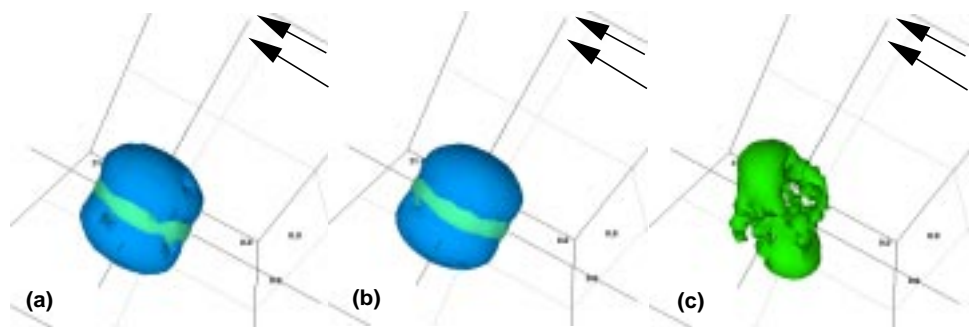


Figure 9.6 Probability isosurfaces. (a) Same isosurface as in Fig. 9.5. (b) Probability isosurface as in Fig. 9.5., except that it was calculated with respect to the original distribution function. (c) Isosurface of the difference between the two B-bead probabilities in Fig. 9.6.a and Fig. 9.6.b. Indicated is a 3 percent deviation. Larger deviations are infrequent.